JOURNAL OF GEOPHYSICAL RESEARCH, VOL. 104, NO. C8, PAGES 18,269–18,280, AUGUST 15, 1999

Combining altimetry with a thermocline model to examine the transport of the North Atlantic

Richard G. Williams and Matthew Pennington

Oceanography Laboratories, University of Liverpool, Liverpool, England, United Kingdom

Abstract. The relationship between sea surface height and transport is explored using a steady, geostrophic, thermocline model. Given an imposed sea surface height (SSH), analytical solutions reveal different patterns for the transport over the interior of a subtropical gyre determined by the background stratification. For no mixed layer or the limit of weak stratification, transport increases more rapidly westward than SSH across a subtropical gyre, whereas in the limit of strong stratification, transport increases linearly with SSH, and streamlines become more orientated from the northwest to southeast. A modified version of the thermocline model is applied to the subtropical gyre of the North Atlantic and uses SSH from TOPEX/Poseidon altimetry and a functional relationship between potential vorticity and density derived from the National Oceanographic Data Center climatology. The model suggests that the transport over the interior of the subtropical gyre reaches 30 ± 13 Sv, which is broadly in accord with the independent Sverdrup estimate from the wind-stress climatology. The transport pattern includes a north-south asymmetry, which is consistent with both the mixed layer and background stratification influencing the solution.

1. Introduction

In principle, the time-mean surface circulation may be estimated from the sea surface height (SSH hereafter) signal measured by satellite altimetry when combined with an estimate of the geoid. In practice, uncertainty in the geoid has limited the ability to estimate the steady circulation. Even when the geoid error is eventually reduced and reliable estimates of the surface circulation are made, there remains the problem of estimating the underlying velocity profile and transport.

In this study, we develop a simplified thermocline model to examine how the transport is connected to a SSH signal. Thermocline balances have been used to understand the ventilation of the thermocline [e.g., *Luyten et al.*, 1983; *Marshall and Nurser*, 1991; *Williams*, 1991], as well as employed in an inverse study for the eastern Atlantic [*Wunsch*, 1994]. Sea surface height is used as a boundary condition in our thermocline model, rather than the traditionally applied Ekman pumping. Our transport estimates ignore the contribution of the flow beneath the main thermocline. The thermocline solutions are obtained for an idealized basin with different background stratification, as well as for the North Atlantic subtropical gyre using TOPEX/Poseidon altimetry (henceforth T/P). The model is used to reveal how the transport is influenced by the presence of the mixed layer and the background stratification. Our thermocline approach complements recent studies combining SSH with in situ hydrography taken along the satellite track [*Challenor et al.*, 1996], melding SSH with hydrography in an inverse model [*Ganachaud et al.*, 1997; *LeGrand et al.*, 1998], or assimilating SSH into a general circulation model [*Stammer et al.*, 1997].

In section 2, we relate SSH, thermocline thickness, and transport to each other and obtain different analytical thermocline solutions, which are controlled by the SSH, background stratification, and mixed layer. In section 3, we apply our model to the subtropical gyre of the North Atlantic using SSH data from T/P and combining with the EGM-96 geoid. Finally, our conclusions are summarized in section 4.

Paper number 1999JC900125.
0148-0227/99/1999JC900125$09.00

2. Relationship Between Sea Surface Height and Transport

2.1. Sea Surface Height and Transport for a Single, Moving Layer

Over the gyre scale, there appears to be a relationship between the upper ocean transport, dynamic sea surface height (SSH) and the thickness of the thermocline: In subtropical gyres, the equatorward transport in the ocean interior is associated with a westward increase in both SSH and thickness of the main thermocline. To illustrate this connection, first consider the

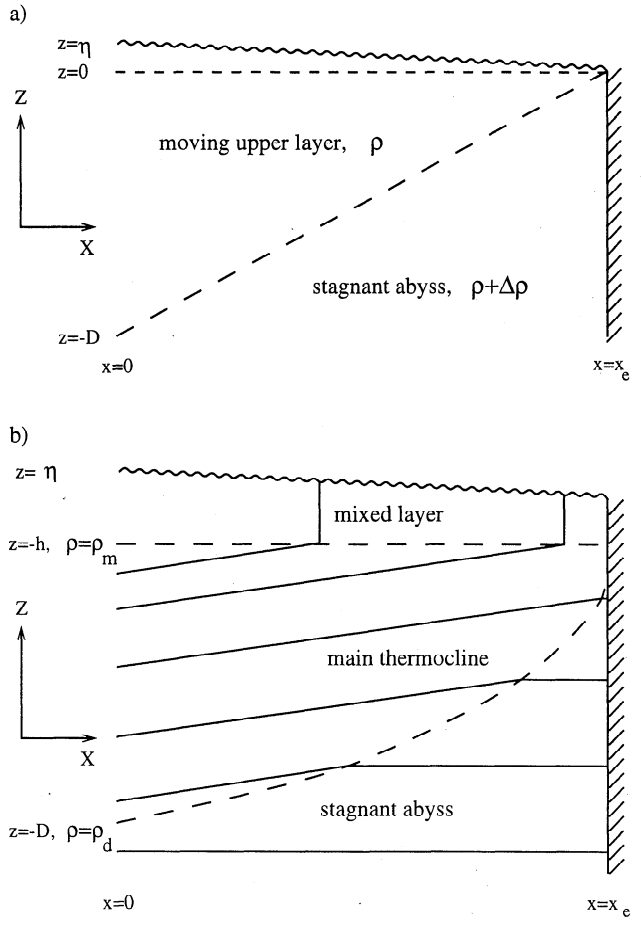

Figure 1. A schematic west-east section for (a) the one and a half layer model and (b) the continuous thermocline model overlying a stagnant abyss. An equatorward transport (in the Northern Hemisphere) is associated with a westward increase in the thickness of the moving layer and sea surface height (exaggerated in the figure). In Figure 1b, isopycnals (solid lines) slope within the thermocline and are horizontal in the abyss; the base of the moving water is depicted by dashed lines. Isopycnals outcrop into a vertically homogeneous mixed layer (whose base is depicted by dashed lines).

most simplified model of a thermocline consisting of a single layer of moving fluid overlying a stagnant abyss (Figure 1a). In this case, the meridional geostrophic velocity v_s depends on the zonal gradients in both SSH, η, and the thickness of the thermocline, D,

$$v_s = \frac{g}{f}\frac{\partial \eta}{\partial x} \tag{1a}$$

$$v_s = \frac{g'}{f}\frac{\partial D}{\partial x}, \tag{1b}$$

and assuming that η and D both vanish on the eastern boundary implies that SSH is linearly related to thermocline thickness:

$$\eta(x) = \frac{g'}{g}D(x). \tag{2}$$

Here the reduced gravity is $g' = g\Delta\rho/\rho$. The transport stream function ψ, defined by $\partial\psi/\partial x = vD$, is related to the square of the thermocline thickness or the square of the SSH signal:

$$\psi(x) = \frac{g'}{2f}D^2(x) = \frac{g^2}{2fg'}\eta^2(x), \tag{3}$$

where ψ is assumed to vanish on the eastern boundary. Assuming that SSH increases westward by ~ 1 m across the subtropical gyre implies that the thermocline deepens westward by ~ 1 km and the equatorward transport reaches ~ 50 Sv (for $f \sim 10^{-4}$ s^{-1} and $g' \sim 10^{-2}$ m s^{-2}).

This simple example illustrates the connection between SSH, thermocline thickness, and transport in the upper ocean. We now extend this single-layer model to a thermocline model with continuous stratification, which leads to a different relationship between SSH and transport. These simplified models assume a steady equilibrium state and ignore any interaction between the flow and the bottom topography.

2.2. Sea Surface Height and Transport for Continuous Stratification

The surface geostrophic velocity is assumed here to depend on the velocity shear integrated over the mixed layer and stratified thermocline (see Figure 1b) with the contribution of the velocity shear below the thermocline neglected. The meridional component of surface velocity is given by

$$v_s = \int_{-D}^{0} \frac{\partial v}{\partial z}\,dz$$

$$v_s = \int_{-h}^{0} \frac{\partial v}{\partial z}\,dz - \int_{\rho_m}^{\rho_d} \frac{\partial v}{\partial \rho}\,d\rho, \tag{4}$$

where the velocity change over the mixed layer and the main thermocline are represented by the first and second terms on the right-hand side with the latter evaluated in density space; h and D are the thickness of the mixed layer and main thermocline, and ρ_m and ρ_d are the density of the mixed layer and base of the main thermocline, respectively.

Assuming thermal-wind balance in the mixed layer and thermocline,

$$\frac{\partial v}{\partial z} = -\frac{g}{\rho_0 f}\frac{\partial \rho}{\partial x} \qquad \frac{\partial v}{\partial \rho} = \frac{g}{\rho_0 f}\frac{\partial Z}{\partial x},$$

then (4) may be written as

$$v_s = -\frac{g}{\rho_0 f}\left(h\frac{\partial \rho_m}{\partial x} + \int_{\rho_m}^{\rho_d}\frac{\partial Z}{\partial x}\,d\rho\right),$$

which may be rearranged to give

$$v_s = -\frac{g}{\rho_0 f}\left(\frac{\partial}{\partial x}\int_{\rho_m}^{\rho_d} Z\,d\rho - Z(\rho_d)\frac{\partial \rho_d}{\partial x}\right). \tag{5}$$

Here, $Z(\rho)$ denotes the vertical position of isopycnals within the thermocline and ρ_0 is a reference density. Density is assumed to be continuous between the moving fluid and the stagnant abyss with $Z(\rho_d) = Z_a(\rho_d)$ at

the base of the thermocline, where $Z_a(\rho)$ is the vertical position of an isopycnal in the stagnant abyss. Applying this matching condition and integrating (1a) and (5) from the eastern boundary at x_e to within the interior at x relates the zonal change in SSH and the interior density field:

$$-\rho_0(\eta(x)-\eta(x_e)) = \int_{\rho_m(x)}^{\rho_d(x)} Z\,d\rho - \int_{\rho_m(x_e)}^{\rho_d(x_e)} Z\,d\rho - \int_{\rho_d(x_e)}^{\rho_d(x)} Z_a\,d\rho.$$

This relation for the SSH variation in x can be combined with an equivalent relation in y to give

$$-\rho_0\,(\eta(x,y)-\eta(x_e,y_s)) = \int_{\rho_m(x,y)}^{\rho_d(x,y)} Z\,d\rho - \int_{\rho_m(x_e,y_s)}^{\rho_d(x_e,y_s)} Z\,d\rho - \int_{\rho_d(x_e,y_s)}^{\rho_d(x,y)} Z_a\,d\rho. \quad (6)$$

The change in SSH depends on the integrated height of isopycnals within the moving water at x (first term on right-hand side) minus the integrated height of isopycnals at the reference point, chosen to be at the southeast corner of the domain at x_e,y_s. The integrated height of isopycnals at the reference point is made up by two contributions from within the moving water and stagnant abyss (second and third terms on right-hand side, respectively). This relationship is analogous to that for the one and a half layer model (equation (2)); when the moving water has vanishing thickness on the eastern boundary and no abyssal stratification, then the second and third terms on the right-hand side of (6), respectively, vanish.

The transport stream function, defined by

$$\frac{\partial\psi}{\partial x} = \int_{-D}^{0} v\,dz \qquad \frac{\partial\psi}{\partial y} = -\int_{-D}^{0} u\,dz,$$

can likewise be related to the structure of the thermocline, where the thermocline thickness is defined by $D=-Z(\rho_d)$. Following section 3d in *Williams* [1989], the transport may be written in terms of the shear within the mixed layer from its horizontal density gradient and the shear from the deformation of the interior density field in the thermocline:

$$\frac{\partial\psi}{\partial x} = -\frac{g}{2\rho_0 f}\left(h^2\frac{\partial\rho_m}{\partial x} + \int_{\rho_m}^{\rho_d}\frac{\partial}{\partial x}Z^2\,d\rho\right)$$
$$\frac{\partial\psi}{\partial x} = -\frac{g}{2\rho_0 f}\left(Z^2(\rho_d)\frac{\partial\rho_d}{\partial x} + \frac{\partial}{\partial x}\int_{\rho_m}^{\rho_d} Z^2\,d\rho\right). \quad (7)$$

Integrating (7) with x gives

$$\frac{2\rho_o f}{g}\,(\psi(x,y)-\psi(x_e,y)) = \int_{\rho_m(x,y)}^{\rho_d(x,y)} Z^2\,d\rho - \int_{\rho_m(x_e,y)}^{\rho_d(x_e,y)} Z^2\,d\rho - \int_{\rho_d(x_e,y)}^{\rho_d(x,y)} Z_a^2\,d\rho. \quad (8a)$$

Note how η and ψ vary in a similar manner in (6) and (8a), with η depending on the integral of the isopycnal height and ψ depending on the integral of the square in the isopycnal height.

An analogous relation is obtained for the variation of ψ with y:

$$\frac{2\rho_o}{g}\int_{y_s}^{y} f\frac{\partial\psi}{\partial y}dy = \int_{\rho_m(x,y)}^{\rho_d(x,y)} Z^2\,d\rho - \int_{\rho_m(x,y_s)}^{\rho_d(x,y_s)} Z^2\,d\rho - \int_{\rho_d(x,y_s)}^{\rho_d(x,y)} Z_a^2\,d\rho, \quad (8b)$$

which is more complicated than (8a) through f varying with y; here, y_s marks the position of the southern boundary. These relations (6), (8a), and (8b) connect the SSH and transport to the interior density structure. They are solved using appropriate boundary conditions for the North Atlantic in section 3, but, first a simplified limit of uniform potential vorticity is considered.

2.3. Transport Relations for Uniform Potential Vorticity

Analytical solutions relating the transport and SSH are now derived with fluid within the thermocline assumed to have uniform potential vorticity,

$$Q_0 = -\frac{f}{\rho_0}\frac{\partial\rho}{\partial z},$$

whereas fluid outside the thermocline is assumed to be stagnant and have a constant stratification, $\partial\rho/\partial z|_a$. Assuming that the potential vorticity is homogenized to the value on the northern boundary of the subtropical gyre (with the same stratification in the moving and stagnant water there) leads to

$$Q_0 = -\frac{f_0}{\rho_0}\left.\frac{\partial\rho}{\partial z}\right|_a,$$

where f_0 is the planetary vorticity on the northern boundary.

The integral relations for SSH, (6), and ψ, (8a) and (8b), can then be evaluated (using $\partial\rho=-\rho_0 Q_0\partial z/f$ in the moving fluid and $\partial\rho=-\rho_0 Q_0\partial z/f_0$ in the stagnant fluid) to give relations for SSH,

$$\eta(x,y) = \frac{Q_0}{2f}\left\{-h^2(x,y)+\left(1-\frac{f}{f_0}\right)D^2(x,y)\right\}, \quad (9)$$

for ψ varying in x,

$$\psi(x,y)-\psi(x_e,y) = \frac{gQ_0}{6f^2}\left\{-h^3(x,y)+h^3(x_e,y) + \left(1-\frac{f}{f_0}\right)\left(D^3(x,y)-D^3(x_e,y)\right)\right\}, \quad (10a)$$

and for ψ varying in y,

$$\psi(x,y) = \frac{gQ_0}{6}\int_{y_s}^{y}\frac{1}{f}\frac{\partial}{\partial y}\frac{1}{f}\left\{-h^3(x,y) + \left(1-\frac{f}{f_0}\right)D^3(x,y)\right\}dy, \tag{10b}$$

where, for simplicity, we assume that the SSH, transport, mixed layer, and bowl all vanish on the southern boundary.

2.4. Idealized Transport Solutions

In order to understand how the transport is related to SSH, consider the following idealized case where the SSH is assumed to vary sinusoidally with y over the basin and increase linearly westward from a zero value on the eastern boundary:

$$\eta(x,y) = \eta_o(1 - x/x_e)\sin(\pi y/L). \tag{11}$$

Here, η_0 is chosen to be 0.5 m. The vanishing in SSH along the eastern boundary requires that there be a compensating velocity shear in the mixed layer and thermocline, which from (9) implies that the bowl and mixed layer thickness are related along the eastern boundary by

$$D^2(x_e,y) = h^2(x_e,y)(1 - f/f_0)^{-1}.$$

Accordingly, (9) and (10a) may be combined to give

$$\psi(x,y) - \psi(x_e,y) = \frac{gQ_0h^3}{6f^2}\left(1-\frac{f}{f_0}\right)^{-1/2}\left\{\left(1+\frac{2f\eta}{Q_0h^2}\right)^{3/2} - 1\right\}, \tag{12}$$

where, for simplicity, the mixed layer thickness is assumed to vary only with y. There are two simplifying cases:

1. For either no mixed layer or the limit of relatively weak stratification, $2f\eta/(Q_0h^2) >> 1$, (12) reduces to

$$\psi(x,y) - \psi(x_e,y) \simeq \frac{g}{3}\left(\frac{2}{fQ_0}\right)^{1/2}\left(1-\frac{f}{f_0}\right)^{-1/2}\eta^{3/2}. \tag{13a}$$

Note that ψ is proportional to $\eta^{3/2}$, rather than η^2, as obtained in the one and a half layer model (equation (3)). Choosing values of $f/f_0 \sim 1/2$, $Q_o = 10^{-10}$ m^{-1} s^{-1}, a SSH change $\eta(x) \sim 1$ m gives a transport of ~ 40 Sv.

2. For the limit of strong stratification or thick mixed layers, $2f\eta/(Q_0h^2) << 1$, applying a Taylor expansion gives a linear relation between ψ and η:

$$\psi(x,y) - \psi(x_e,y) \simeq \frac{gh\eta}{2f}\left(1-\frac{f}{f_0}\right)^{-1/2}. \tag{13b}$$

We now obtain analytical solutions to (12) in order to illustrate the different limits using plausible stratifications for a subtropical gyre. The transport solutions are obtained for the interior of a subtropical gyre in a rectangular basin; the basin is centered along 30°N and extends 60° in longitude and 30° in latitude, and a beta-plane approximation is employed, $f = f_0 - \beta(L - y)$, with f_0 being the value on the northern boundary at L and β, the planetary vorticity gradient. The same boundary conditions for SSH and mixed layer thickness are employed, but the background stratification is altered; the mixed layer thickness is chosen to linearly vary with y from a zero value on the southern boundary to 300 m on the northern boundary. The Ekman vertical velocity w_e is diagnosed from the transport solutions using

$$w_e = \frac{\beta}{f}\frac{\partial\psi}{\partial x}.$$

For relatively weak stratification, $Q_0 = 10^{-10}$ m^{-1} s^{-1}, the SSH variation given in (11) is associated with a classical subtropical gyre recirculation with a volume transport reaching 35 Sv (Figure 2a); note that an implicit western boundary current is required to supply and receive fluid to the northern and southern halves of the gyre interior, respectively. The southward flow is more intense on the western side of the basin, consistent with the ψ variation with x being proportional to $\eta^{3/2}$. In this solution, the nondimensional ratio, $2f\eta/(Q_0h^2) \sim 25$, with the solution being similar to the no mixed layer or low stratification limit of (13a). The Ekman pumping reaches a maximum value of 70 m yr^{-1} at the western side of the center of the gyre (Figure 2b). The thickness of the thermocline increases westward and northward, reaching a maximum of 2.5 km at the northwest corner, away from the zero value along the southern boundary (Figure 2c).

For a relatively strong stratification, $Q_0 = 10^{-9}$ m^{-1}s^{-1}, the transport solution changes character. The recirculation weakens with a more linear variation of ψ with x across the basin and a stronger inflow from the eastern boundary (Figure 3a). This solution approaches the linear variation shown in (13b), although $2f\eta/(Q_0h^2) \sim 2.5$. The Ekman pumping is weaker, reaching only 25 m yr^{-1}, and the thermocline is thinner reaching maximum values of only 1.5 km (Figures 3b and 3c).

In summary, the relationship between the SSH and transport over the subtropical gyre varies according to the relative magnitude of the SSH signal to the product of the background stratification and mixed layer thickness. We now examine how relevant these contrasting limits are to the North Atlantic.

3. Thermocline Model Constrained by T/P Altimetry

The thermocline model is now applied to the North Atlantic subtropical gyre using more realistic boundary conditions than applied for the previous idealized basin.

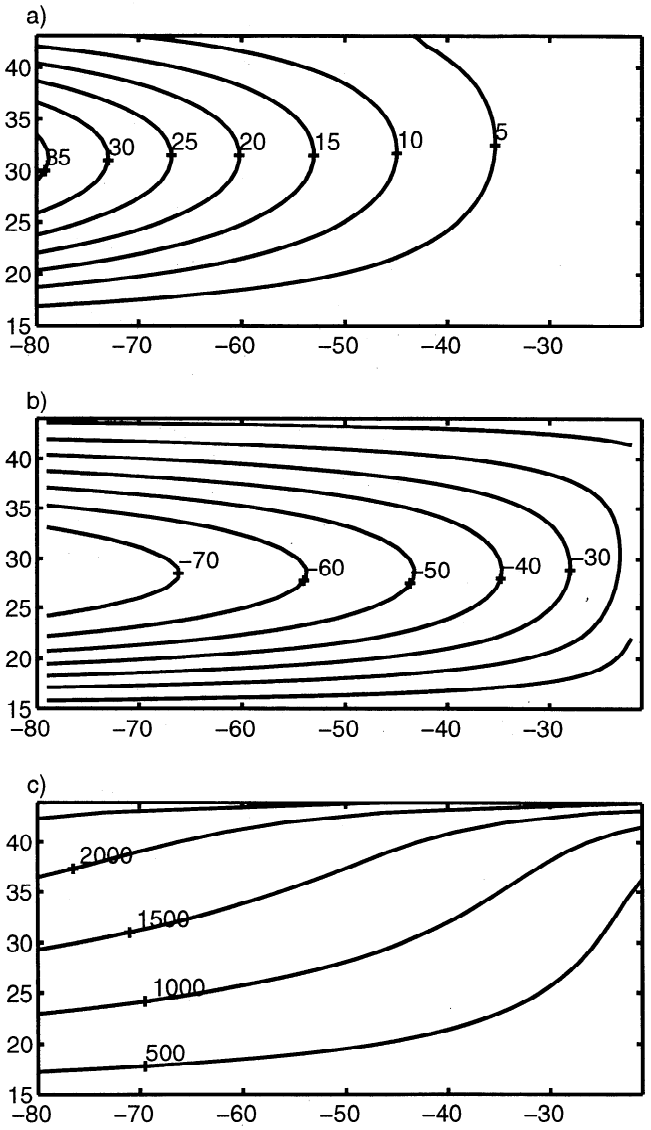

Figure 2. Analytical solutions of the thermocline model to an imposed sea surface height (SSH) distribution, $\eta_0(1 - x/x_e)\sin(\pi y/L)$, with uniform low Q_0 of 10^{-10} m^{-1} s^{-1}: (a) the transport stream function (Sv); (b) the Ekman vertical velocity (m yr^{-1}); and (c) the thermocline thickness (m).

3.1. SSH Signal Over the North Atlantic

The SSH signal is shown in Figure 4 from a time mean of 5 years of TOPEX data from October 1992 to September 1997. The EGM-96 geoid [*Lemoine et al.*, 1999] and standard environmental corrections are applied [*Callaghan*, 1993], including the CSR 3.0 tide model and the inverse barometer correction, with the data binned into land free, 1° squares and any residual SSH with a modulus greater than 150 cm removed.

The Gulf Stream/North Atlantic Current signal is evident in the band of enhanced SSH gradients running northeastward from 75°W, 35°N to 40°W, 45°N. The subtropical and subpolar gyres are evident by the broadly anticyclonic and cyclonic circulations occurring south and north, respectively, of the North Atlantic Current. There appears to be much fine scale structure, which might possibly represent real ocean currents or geoid errors.

As our focus is on the gyre-scale circulation, we choose to smooth the SSH signal using a short-wavelength filter (using an exponential weighting extending over a radius of 3°). The resulting smoothed SSH is shown in Figure 4b. The subtropical gyre is now clearly revealed with equatorward flow occurring over much of the North Atlantic and with a closed anticyclonic circulation west of 50°W; SSH increases westward over the gyre interior, reaching a maximum value of 60 cm at 60°W, 25°N. The subpolar gyre (not shown) is relatively confined to north of 50°N; SSH decreases westward over the gyre interior, reaching −60 cm at 50°W,

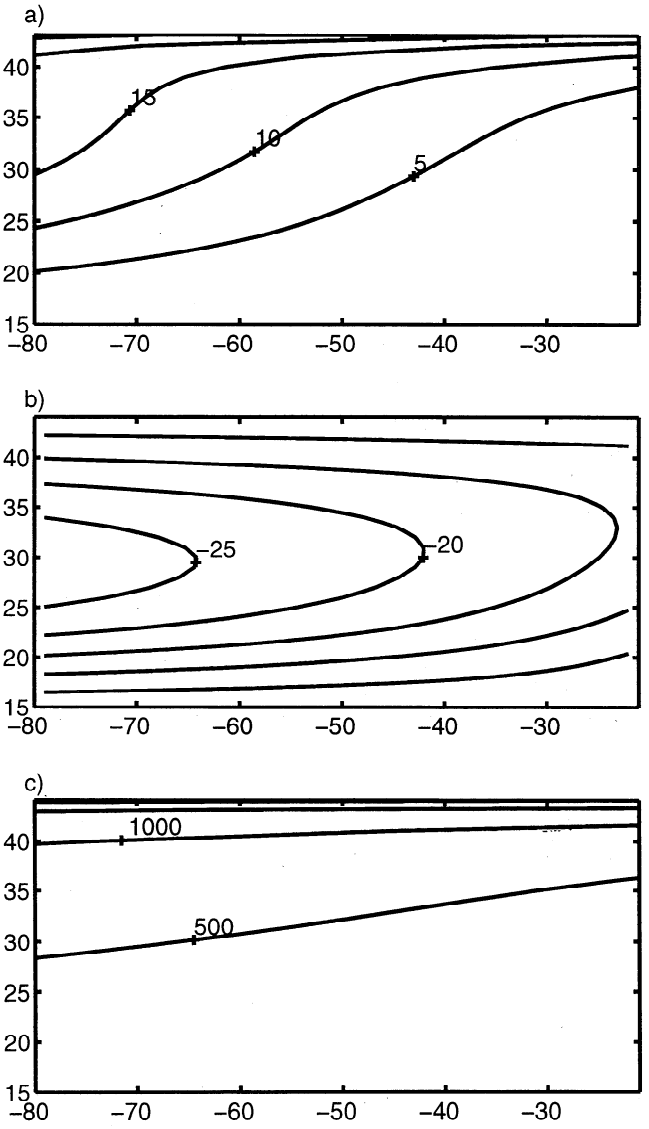

Figure 3. Analytical solutions of the thermocline model to an imposed sea surface height (SSH) distribution, $\eta_0(1 - x/x_e)\sin(\pi y/L)$, with uniform high Q_0 of 10^{-9} m^{-1} s^{-1}: (a) the transport stream function (Sv); (b) the Ekman vertical velocity (m yr^{-1}); and (c) the thermocline thickness (m).

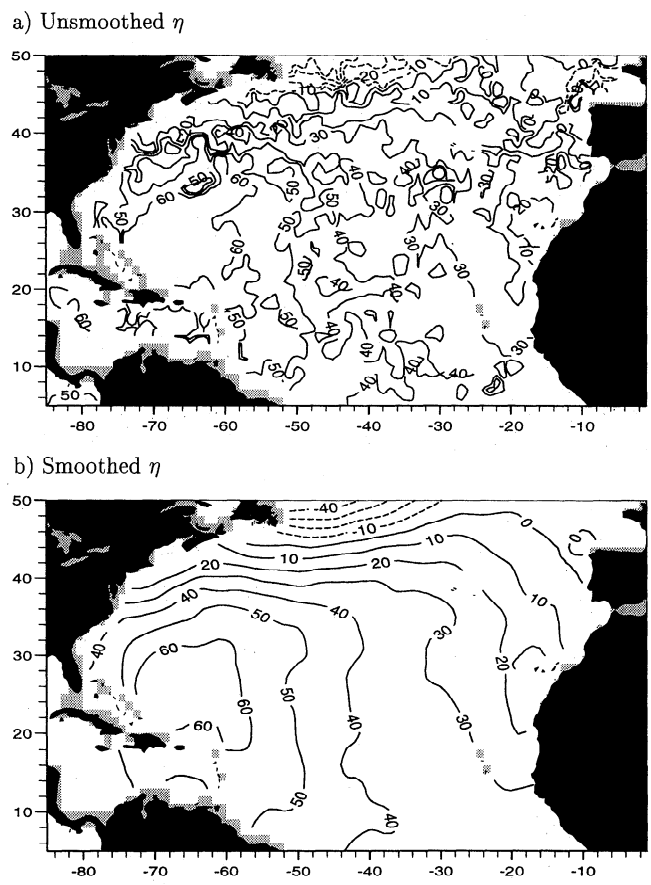

Figure 4. The mean SSH (cm) taken from 5 years TOPEX/Poseidon (T/P) data from October 1992 to September 1997 using the EGM-96 geoid: (a) with no smoothing and (b) with smoothing.

55°N. These gyre signals are persistent features over the 5 year period of T/P data and dominate seasonal and interannual changes, which typically reach ±8 cm and ±4 cm, respectively. The North Atlantic Current appears to be much wider than the 100 km which is typically observed. This over-diffuse signal is partly a result of our processing: The original T/P data is binned in 1° squares, with a 5 year time average, and the spatial smoothing is applied.

Our objective now is to estimate the transport associated with the smoothed SSH field using our thermocline model and examine how the solution is controlled by the background stratification.

3.2. Potential Vorticity Variation With Density

The thermocline solutions for the idealized subtropical gyre revealed how the transport stream function varied with the background stratification. Accordingly, we now derive the $Q(\rho)$ relationship using bottle data from the National Oceanographic Data Center (NODC) climatology over the North Atlantic from 10°N to 40°N and 80°W to 10°W following the algorithm described by *O'Dwyer and Williams* [1997]. The $Q(\rho)$ relationship beneath the winter mixed layer is shown in Figure 5. The mean Q decreases by an order of magnitude from typically 10^{-9} m^{-1} s^{-1} at $\sigma = 25$ to 10^{-10} m^{-1} s^{-1} at $\sigma = 27$. The standard error is relatively small, suggesting that an accurate mean is evaluated, but the standard deviation is large for lighter isopycnals. The thermocline model is next used to examine the high and low Q limits with T/P data and then extended to use the more realistic, derived functional relationship $Q(\rho)$ in section 3.4. This choice of assuming uniform Q along an isopycnal should be viewed as a device to obtain thermocline solutions (as has been applied in other thermocline studies [e.g., *Marshall and Nurser,* 1991]). Thermocline studies by *Williams* [1991] suggest that changes in Q subducted from different mixed layer distributions over the subtropical gyre lead only to relatively minor changes in the large-scale flow pattern.

3.3. Analytical Thermocline Solutions With Constant Potential Vorticity

The sensitivity of the transport to the background potential vorticity is investigated using the analytical thermocline model developed in section 2.3 but now using more realistic boundary conditions than applied in section 2.4. SSH is taken from T/P (Figure 4b), and the winter mixed layer thickness is taken from climatology (Figure 7a) (discussed further in section 3.4). Analytical solutions are obtained for different choices in Q_0 together with changes in the reference thermocline thickness. The model algorithm solves for $D(x, y)$ and $\psi(x, y)$ using the imposed $\eta(x, y)$ and $h(x, y)$ fields by, first, solving along the eastern boundary, using (9) and (10b) after imposing the reference thermocline thickness at 15°N, 20°W, and, second, solving in the interior using (9) and (10a).

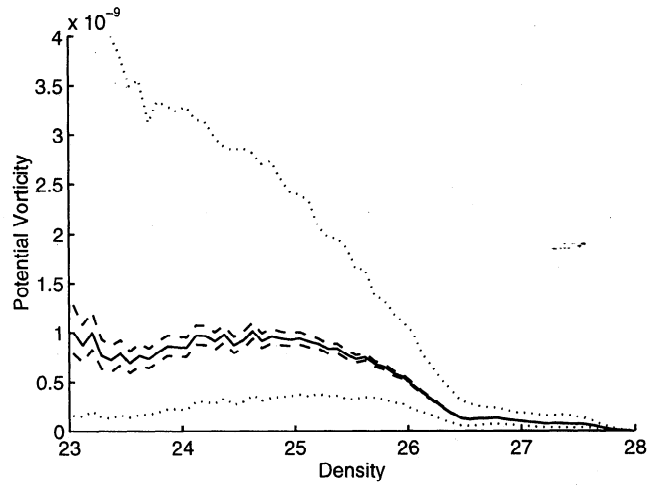

Figure 5. Potential vorticity Q (10^{-9} m^{-1} s^{-1}) versus density (kg m^{-3}) evaluated using bottle data from the National Oceanographic Data Center climatology over the North Atlantic from 10°N to 40°N and 80°W to 10°W. The geometric mean, standard error, and standard deviation are shown by the solid, dashed, and dotted lines, respectively.

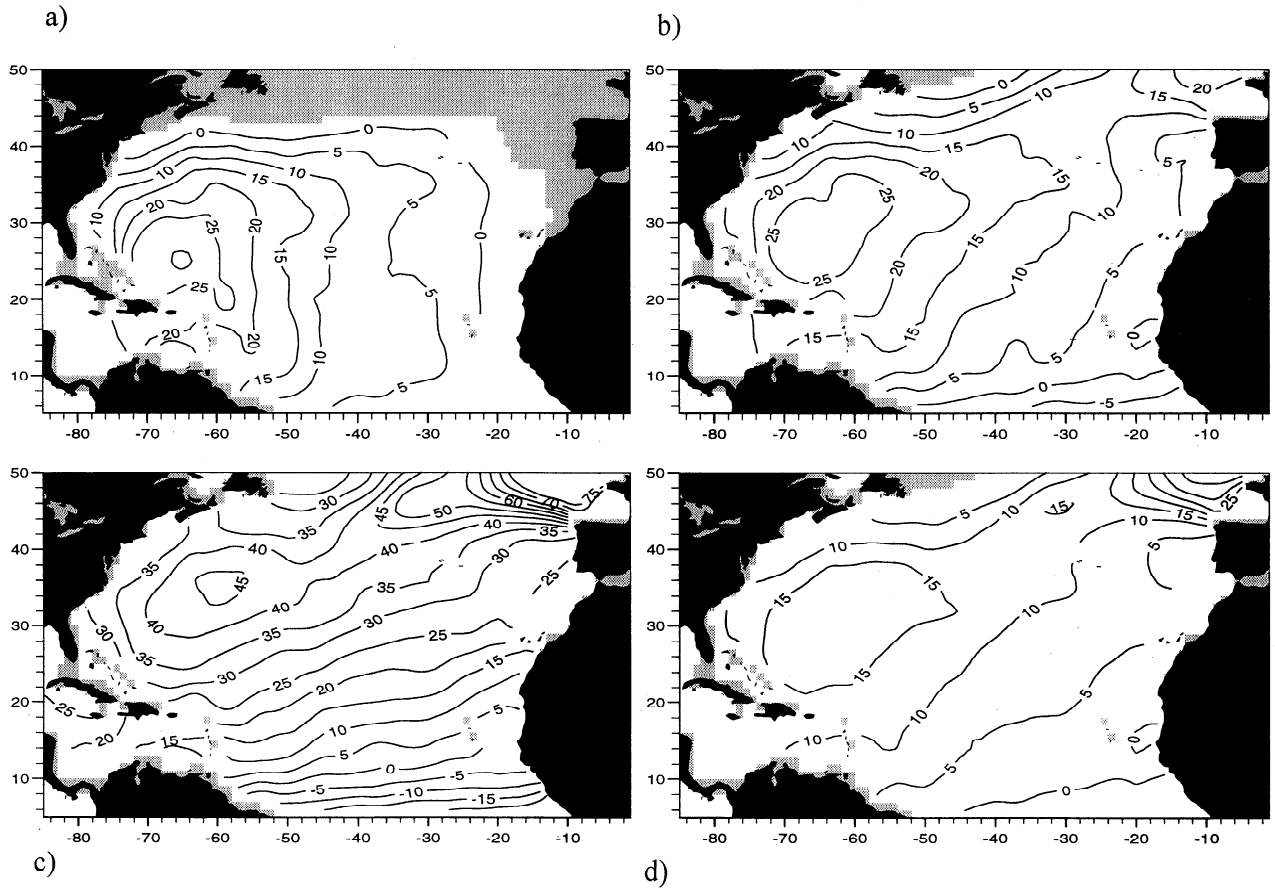

Figure 6. Analytical solutions for the transport stream function (Sv) using mean SSH from T/P and uniform potential vorticity: (a) low Q of 10^{-10} m^{-1} s^{-1}, (b) intermediate Q of 4×10^{-9} m^{-1} s^{-1} and (c) high Q of 10^{-9} m^{-1} s^{-1} (the unshaded area represents the solution domain); a reference thermocline thickness of 400 m is imposed at 15°N, 20°W. In addition, (d) a solution with a reduced thermocline thickness of 250 m is included for high Q.

In the limit of a low Q_0 of 10^{-10} m^{-1} s^{-1}, there is again an anticyclonic circulation reaching 25 Sv with meridional streamlines over most of the subtropical gyre (Figure 6a). As Q_0 is increased to 4×10^{-10} m^{-1} s^{-1} and 10^{-9} m^{-1} s^{-1}, the circulation becomes less symmetric with latitude and streamlines become more orientated from the northwest to southeast (Figures 6b and c). The west-east contrast in transport across the basin reduces as Q_0 increases, which is also obtained in the low and high Q limits for the idealized subtropical gyre (shown in Figures 2 and 3). However, there is now an additional volume flux from the eastern boundary, which becomes unrealistically large for high Q. Along the eastern boundary of the model, the thermocline thickness $D(x_e, y)$ increases poleward following (9) as $h(x_e, y)$ increases and $\eta(x_e, y)$ decreases (previously $\eta(x_e, y) = 0$ in section 2.4). The velocity shear associated with the poleward increase in $D(x_e, y)$ leads to a westward volume flux from (10b). When the reference thermocline thickness (set at 15°N, 20°W) is reduced from 400 m for the above cases to 250 m, this westward volume flux reduces, although the streamlines still retain their northeast to southwest orientation (Figure 6d).

We now extend the thermocline model to include the $Q(\rho)$ profile following that derived from climatology (Figure 5) in order to examine the relevance of the solutions with uniform high or low Q.

3.4. Thermocline Solutions With Variable Potential Vorticity

Thermocline model solutions for a variable $Q(\rho)$ profile are now obtained by numerically solving the controlling equations (6), (8a), and (8b) developed in section 2.2, which connect the SSH and transport variations to the interior density structure. The model uses boundary conditions from the imposed T/P data, the variable $Q(\rho)$ relationship inferred from NODC data, and the thickness of the mixed layer (as shown in Figures 4b, 5 and 7a, respectively). The model algorithm again involves solving for the thermocline thickness and transport, first, along the eastern boundary using (6) and (8b) and, second, zonally into the interior using (6) and (8a); further details are described by *Williams* [1991] and *Pennington* [1998]. The only arbitrary parameter, the reference thermocline thickness, is chosen to be 500 m at 15°N, 20°W in order to make the east-

ward transport approach zero over the domain across 20°W. The solutions are compared with the climatology inferred from *Levitus and Boyer* [1994] and *Levitus et al.* [1994] (henceforth referred to as the Levitus climatology).

3.4.1. Mixed layer. The thickness of the winter mixed layer is chosen as an upper boundary condition for the thermocline model in order to avoid the seasonal thermocline, where there are large Q contrasts along isopycnals, as shown by *Stammer and Woods* [1987]. In addition, fluid is directly transferred from the mixed layer to the main thermocline only at the end of winter [*Stommel*, 1979; *Williams et al.*, 1995].

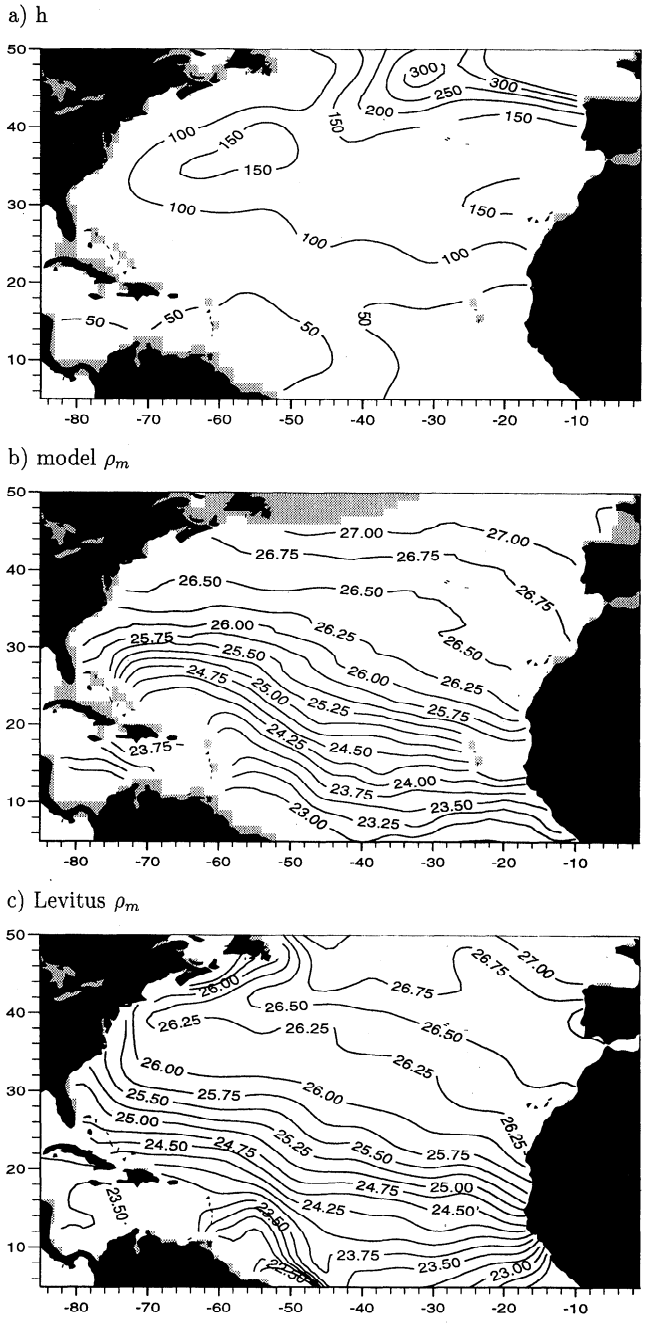

Figure 7. (a) The mixed layer thickness (m) in winter derived from the Levitus climatology (and used as a boundary condition in the thermocline model); (b) the surface density (kg m^{-3}) solved for in the thermocline model (with the unshaded area representing the solution domain); and (c) the surface density in winter derived from the Levitus climatology.

The thickness of the winter mixed layer is shown in Figure 7a and is diagnosed from the Levitus climatology for the months of January to March; the base of the mixed layer is defined by where the potential density increases by 0.125 kg m^{-3} from the surface. The surface density in the model is shown in Figure 7b and is broadly similar to the Levitus climatology for winter (Figure 7c). The solutions do differ near the Gulf Stream, where the observed mixed layer density shows an advective signal, which is not incorporated in the thermocline model. This solution depends on the SSH slope and the imposed $Q/(\rho)$ relationship and only to a lesser extent on the mixed layer thickness when it becomes thick toward the northern boundary.

3.4.2. Transport. The transport in the model is evaluated from the isopycnal slopes by integrating the thermal-wind equations with the boundary condition of no flow at the base of the thermocline. A map of the model transport over the subtropical gyre is shown in Figure 8a. The anticyclonic circulation over the whole basin reaches 25 Sv with a further 5 Sv concentrated in a localized recirculation centered around 60°W, 34°N.

The transport stream function resembles aspects of the previous analytical solutions with constant Q. The maximum transport is close to that obtained in the analytical model with low Q or no mixed layer (Figure 6a). However, the transport streamlines are orientated from the northeast to the southwest over the eastern half of the domain, which is similar to the higher Q cases shown in Figures 6b and 6c. Consequently, the transport solution is influenced by the value of the background stratification and presence of the mixed layer. The transport solutions show a closing off of streamlines near the western boundary. This signature is a consequence of the SSH variation from T/P (see Figure 4), which is not seen in the analytical solutions using an idealized SSH (Figures 2 and 3). However, in reality, this signal is probably associated with higher-order dynamics not incorporated in the model, such as changes in Q along isopycnals or relative vorticity becoming important. The implied Ekman pumping obtained from differentiating the transport stream function gives a plausible midbasin value of typically 60 m yr^{-1}, but with noisy, unrealistically large variations of ±40 m yr^{-1} over horizontal scales of 500 km.

The model obtains a transport solution only where the main thermocline exists. The thermocline thickness is shown in Figure 8b and deepens to the west, reaching 1500 m at 55°W, 35°N, which is reminiscent of the analytical solutions. Over the subpolar gyre, the main thermocline thins westward until the thermocline eventually vanishes with its base outcropping into the mixed layer (along the line where the meridional trans-

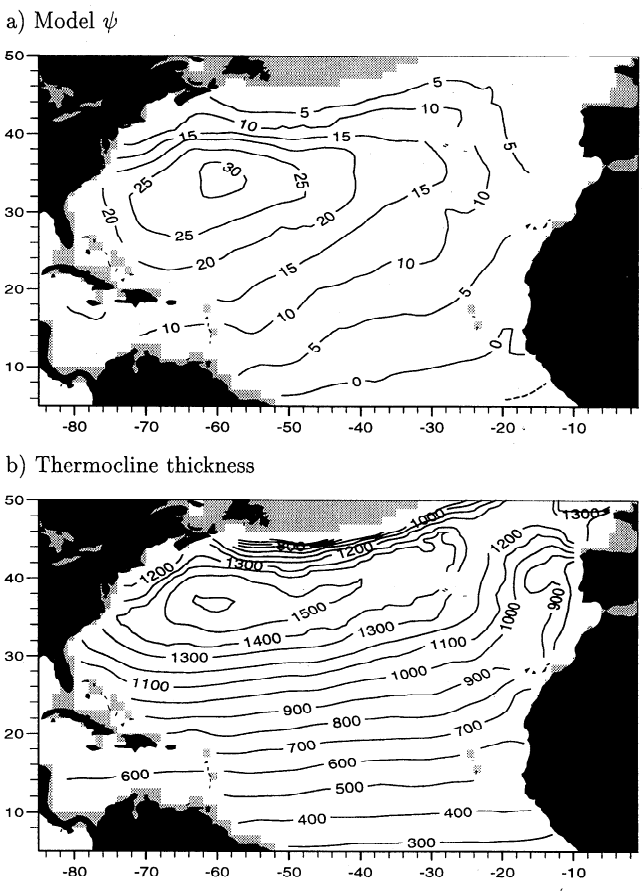

Figure 8. Thermocline model solutions for (a) the transport stream function (Sv) and (b) the thickness of the thermocline (m). The model uses imposed T/P data, a variable potential vorticity inferred from NODC data, and a winter mixed layer thickness (as shown in Figures 4b, 5, and 7a, respectively).

port changes sign). When the thermocline outcrops, the model cannot obtain a solution consistent with the assumption of uniform abyssal stratification; in reality, the thermocline is more seasonal and the flow is more topographically controlled over the subpolar gyre.

3.4.3. Hydrographic sections. The vertical positions of isopycnals are solved for in the thermocline model and are compared with zonal sections from the Levitus climatology (Figure 9 with solid and dashed lines for the model and Levitus, respectively). The gross structure is similar in both the model and climatology: Isopycnals deepen westward in each case by typically 200 m along 36°N and 100 m along 24°N. The thermocline likewise deepens westward, with its base marked by the bottom dotted line in Figure 9.

Along meridional sections at 50°W and 20°W, isopycnals are subducted from the mixed layer to the north, initially deepen, and then shallow to the south (Figures 10a and 10b) in both the model and the climatology. The isopycnal spacing in the model decreases equatorward in order to satisfy potential vorticity conservation. The reversal in isopycnal slope leads to ψ, reaching 27 Sv at 50°W and 7 Sv at 20°W, between 30°N and 40°N, with eastward transport to the north and a return westward transport to the south (Figure 10c). The model does not predict an overall eastward transport over the whole domain at 20°W, although that is suggested from the Levitus climatology (dashed line in Figure 10c) and by *Arhan et al.* [1994], who diagnose an eastward transport of 8.5 Sv crossing 15°W between 20°N and 60°N.

3.4.4. Climatological estimates of transport. Our transport estimates (Figure 8a) are now compared with other independent transport estimates inferred from climatological wind stress and hydrography. A Sverdrup estimate of the geostrophic transport using

$$\frac{\partial \psi}{\partial x} = \frac{f}{\beta \rho} \nabla \times (\tau / f) \tag{14}$$

is estimated using the wind stress τ from the *Isemer and Hasse* [1987] climatology. The Sverdrup estimate reveals an anticyclonic circulation extending from 10°N to 50°N with the maximum transport reaching 35 Sv at 28°N, 75°W (Figure 11a); note that this map does not include horizontal Ekman transport. The geostrophic transport is also estimated from the Levitus climatology by integrating thermal-wind balance from a level of no motion at 2 km. The subtropical gyre appears weaker

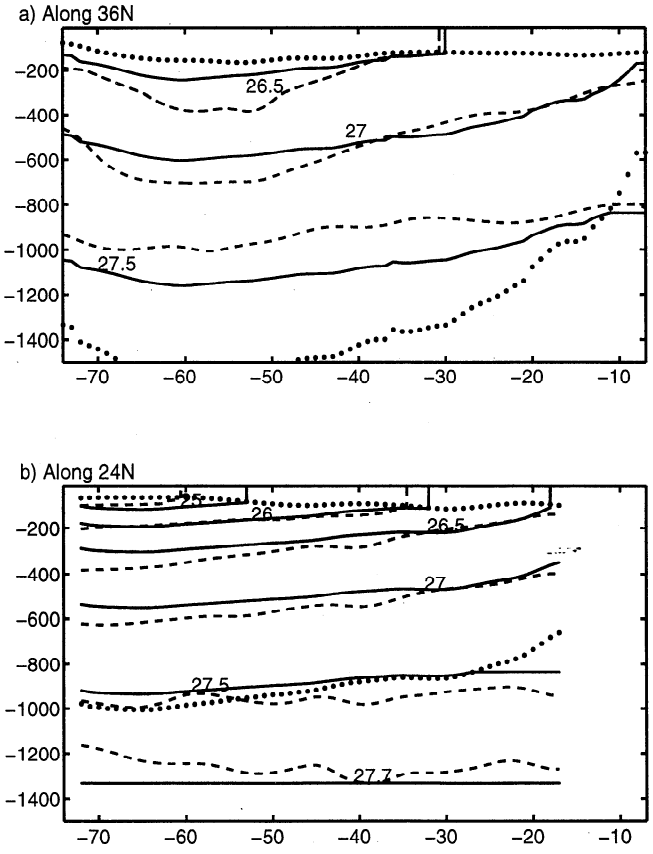

Figure 9. Zonal sections showing isopycnals from the thermocline model (solid line) and Levitus climatology (dashed line) along (a) 36°N and (b) 24°N. The winter mixed layer and base of the thermocline are marked by the top and bottom dotted lines, respectively.

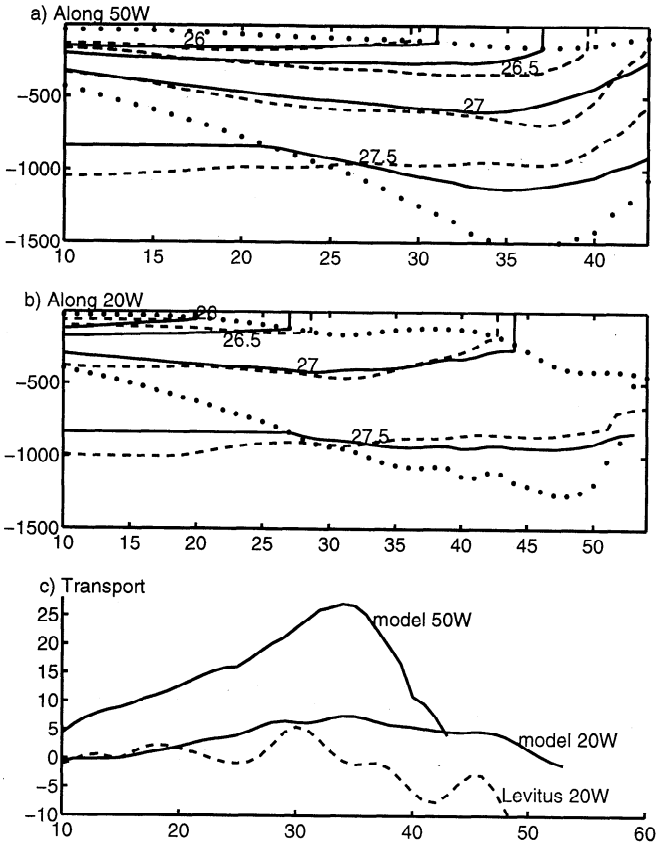

Figure 10. Meridional sections showing isopycnals from the thermocline model (solid line) and Levitus climatology (dashed line) along (a) 50°W and (b) 20°W; the winter mixed layer and base of the thermocline are marked by the top and bottom dotted lines, respectively. The transport stream function (Sv) versus latitude is shown in Figure 10c from the model (solid line) and along 20°W implied from the Levitus climatology (dashed line).

with a maximum transport of 20 Sv and extends only from typically 15°N to 38°N (Figure 11b).

Our thermocline model and climatological estimates all indicate a southward transport across 36°N and 24°N over the interior of the basin (Figure 12). Across 36°N, the model transport reaches 32 Sv at 60°W, compared with lower values of 15 Sv from Sverdrup balance and 20 Sv from the Levitus climatology. Across 24°N, the model transport reaches 21 Sv at 64°W, compared with a higher value of 28 Sv from Sverdrup balance and a lower value of 16 Sv from the Levitus climatology.

In comparison, *Schmitz and McCartney* [1993] review the transport of thermocline waters (warmer than 7°C) and conclude that the Gulf Stream transport is 30 Sv at Florida Strait with 17 Sv supplied from the interior of the subtropical gyre. Farther to the north, the Gulf Stream transport intensifies with intense recirculating cells, reaching 30 Sv. Our transport estimates in Figure 8a show some similar features with 20 Sv supplied to the Gulf Stream off Florida Strait but with the Gulf Stream strengthening to the north by only a further 5 Sv to 10 Sv.

Our thermocline model underestimates the transport of the Gulf Stream owing to ignoring of the strong recirculating, depth-independent flows observed there [*Hogg*, 1992]. The relevance of our transport estimates to the ocean interior likewise depends on the potentially important contribution of the flow beneath the thermocline. This issue has been raised in the debate as to the relevance of the Sverdrup balance [*Wunsch and Roemmich*, 1985]. Direct transport estimates appear to match that predicted by Sverdrup balance east of 55°W and 60°W along 24°N [*Roemmich and Wunsch*, 1985]; also, see *Leetma et al.* [1977] and *Schmitz et al.* [1992]. However, an inverse study by *Paillet and Mercier* [1997] argues that the transport is instead greatly enhanced above the Sverdrup estimate over the eastern Atlantic.

3.5. Sensitivity of the Transport to Model Inputs

The sensitivity of the model estimates of the meridional transport across 36°N is now assessed.

The uncertainty in SSH arising from the geoid is assessed by including an additional west east change of ±15 cm across the entire basin (applied with a uniform gradient from 84°W to 1°W). This change is in accord

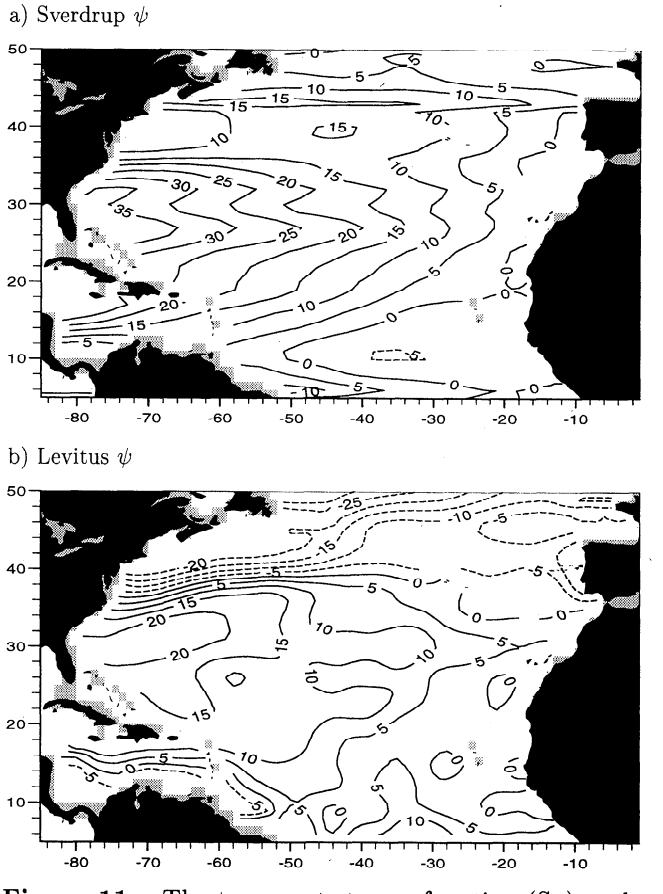

Figure 11. The transport stream function (Sv) evaluated from (a) Sverdrup balance using the wind stress from the *Isemer and Hasse* [1987] climatology and (b) integrating thermal-wind balance with the Levitus climatology, assuming a level of no motion of 2000 m.

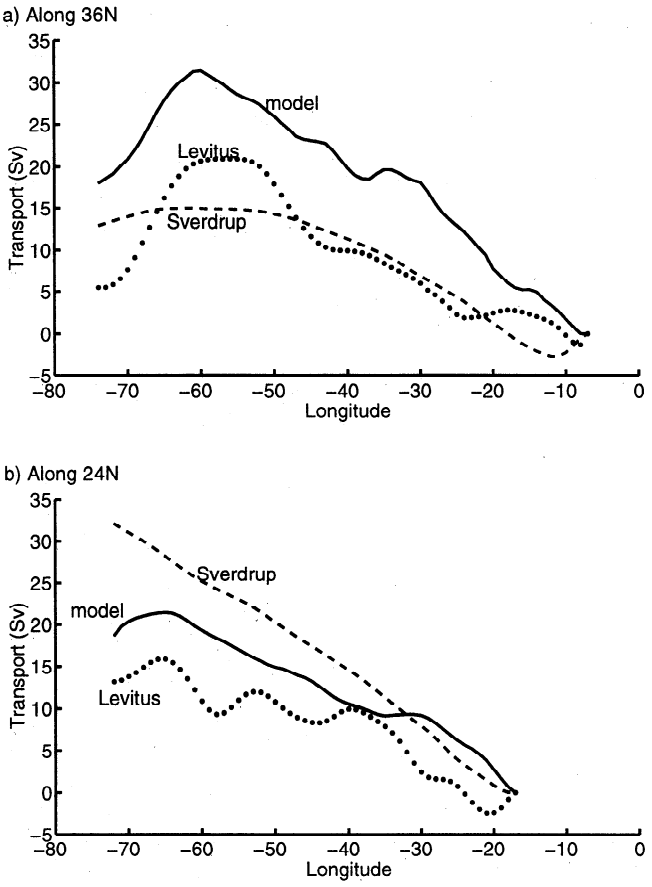

Figure 12. Meridional transport stream function (Sv) from the thermocline model (solid line), Sverdrup balance using the Isemer and Hasse climatology (dashed line), and inferred from the Levitus climatology (dotted line) along (a) 36°N and (b) 24°N.

with the error of the earlier JGM-2 geoid [*Tapley et al.*, 1994] estimated to reach 10-15 cm at a horizontal scale of 1600 km and to decrease further with larger scales. The resulting transport change reaches ±5 Sv at 60°W along 36°N. This transport change from the model is less than that predicted for a barotropic response over the whole fluid column since the transport is carried within the thermocline with a thickness reaching only up to 2 km.

The uncertainty in the $Q(\rho)$ profile used in the thermocline model is assessed by changing $Q(\rho)$ within the moving thermocline by ±5 standard errors as measured from the NODC data (Figure 5), which leads to a transport change of ±4 Sv along 36°N. An uncertainty in the reference thermocline thickness of ±50 m from the chosen value of 500 m leads to a meridional transport change of ±4 Sv across 36°N. Incorporating plausible errors in the winter mixed layer thickness leads to relatively small changes in the transport magnitude.

The total error ranges from ±13 Sv to ±8 Sv according to whether the separate errors are assumed to combine in a systematic or random manner. However, this error range does not include additional errors arising from assumptions made within the model, such as ignoring the flow interacting with the bottom topography.

4. Conclusions

A thermocline model is used to understand the relationship between sea surface height (SSH) and transport over the upper ocean. The character of the transport solutions is found to vary according to the background stratification and presence of a mixed layer. In the limit of no mixed layer or low stratification, the stream function increases rapidly to the west with increasing SSH and is broadly symmetrical with latitude over a subtropical gyre. In the limit of high stratification, the transport increases only linearly westward with SSH, and streamlines become orientated from the northeast to southwest.

The sea surface height from T/P over a 5 year period reveals the surface signature of the quasi-permanent gyre recirculations. We estimate that the transport associated with the T/P signal reaches 30 ± 13 Sv using the thermocline model, which is broadly consistent with the classical Sverdrup estimate from the wind-stress curl. The transport pattern includes streamlines orientated from the northeast to southwest, which suggests that the transport is influenced by the presence of the mixed layer and the background stratification. Our transport estimates have to be viewed with caution because of the neglect of any contribution from the velocity shear below the main thermocline. The relevance of this thermocline model is equivalent to the debate concerning the validity of the Sverdrup balance, which likewise neglects the interaction of the flow with bottom topography. Sverdrup balance over the subtropical gyre has been supported from direct observations and climatological studies [*Leetma et al.*, 1977; *Roemmich and Wunsch*, 1985; *Schmitz et al.*, 1992] but is contradicted by scale analysis and an inverse study for the eastern Atlantic [*Wunsch and Roemmich*, 1985; *Paillet and Mercier*, 1997].

While the thermocline balances include approximations, such as not including time-dependence or relative vorticity, we believe that these balances are useful in understanding how the transport is controlled by the altimetric signals. In particular, our simplified approach may prove useful in understanding the behavior of more complex models used to assimilate altimetric data.

Acknowledgments. This study was supported by a PhD studentship GT93/31/64/91 and a research grant GST/02/1686 from the U.K. Natural Environment Research Council. We are grateful for assistance from Phil Woodworth and for comments by Alex Ganachaud, Keith Haines, Harry Leach and an anonymous reviewer.

References

Arhan, M., A. Colin de Verdière, and L. Mémery, The eastern boundary of the subtropical North Atlantic, *J. Phys. Oceanogr., 24,* 1295–1316, 1944.

Callaghan, P. S., TOPEX/POSEIDON NASA GDR Users Handbook, *JPL Publ. D-8590,* rev. C, Jet Propul. Lab., Pasadena, Calif., 1993.

Challenor, P. G., J. F. Read, R. T. Pollard, and R. T. Tokmakian, Measuring surface currents in Drake Passage from altimetry and hydrography, *J. Phys. Oceanogr., 26,* 2748–2759, 1996.

Ganachaud, A., C. Wunsch, M.-C. Kim, and B. Tapley, Combination of TOPEX/POSEIDON data with a hydrographic inversion for determination of the oceanic general circulation and its relation to geoid accuracy, *Geophys. J. Int., 128,* 708–722, 1997.

Hogg, N. G., On the transport of the Gulf Stream between Cape Hatteras and the Grand Banks, *Deep Sea Res., Part A, 39,* 1231–1246, 1992.

Isemer, H. J., and L. Hasse, *The Bunker Climate Atlas of the North Atlantic Ocean, vol. 2, Air-Sea Interaction,* 252 pp., Springer-Verlag, New York, 1987.

Leetma, A., P. Niiler, and H. Stommel, Does the Sverdrup relation account for the mid-Atlantic circulation?, *J. Mar. Res., 35* 1–9, 1977.

LeGrand, P., H. Mercier, and T. Reynaud, Combining T/P altimetric data with hydrographic data to estimate the mean dynamic topography of the North Atlantic and improve the geoid, *Ann. Geophys., 16,* 638–650, 1998.

Lemoine, F., et al., The development of the NASA GSFC and NIMA Joint Geopotential Model, in *Proceedings of the International Symposium on Gravity, Geoid and Marine Geodesy,* edited by H. Fujimoto, in press, Springer-Verlag, New York, 1999.

Levitus, S., and T. P. Boyer, *World Ocean Atlas 1994,* vol 4, *Temperature, NOAA Atlas NESDIS 4,* 117 pp., Natl. Oceanic and Atmos. Admin., Silver Spring, Md., 1994.

Levitus, S., R. Burgett, and T. P. Boyer, *World Ocean Atlas 1994,* vol 3, *Salinity, NOAA Atlas NESDIS 3,* 99 pp., Natl. Oceanic and Atmos. Admin., Silver Spring, Md., 1994.

Luyten, J. R., J. Pedlosky, and H. Stommel, The ventilated thermocline, *J. Phys. Oceanogr., 13,* 292–309, 1984.

Marshall, J. C., and A. J. G. Nurser, A continuously stratified thermocline model incorporating a mixed layer of variable depth and density, *J. Phys. Oceanogr., 21,* 1780–1792, 1991.

O'Dwyer, J. E., and R. G. Williams, The climatological distribution of potential vorticity over the abyssal ocean, *J. Phys. Oceanogr., 27,* 2488–2506, 1997.

Paillet, J., and H. Mercier, An inverse model of the eastern North Atlantic general circulation and thermocline ventilation, *Deep Sea Res., Part 1, 44,* 1293-1328, 1997.

Pennington, M., Calculating the general circulation of the North Atlantic from TOPEX/POSEIDON using a thermocline model, Ph.D. thesis, Univ. of Liverpool, Liverpool, England, 1998.

Roemmich, D., and C. Wunsch, Two transatlantic sections: meridional circulation and heat flux in the subtropical North Atlantic Ocean, *Deep Sea Res., Part A, 32* 619–664, 1985.

Schmitz, W. J., Jr., and M. S. McCartney, On the North Atlantic circulation, *Rev. Geophys., 31* (1), 29–49, 1993.

Schmitz, W. J., Jr., J. D. Thompson and J. R. Luyten, The Sverdrup circulation for the Atlantic along 24°N, *J. Geophys. Res., 97,* 7251–7256, 1992.

Stammer, D., and J. D. Woods, Isopycnic potential vorticity atlas of the North Atlantic Ocean — Monthly mean maps, *Ber. Inst. Meereskd. Christian-Albrechts-Univ. Kiel, 165,* 108 pp., 1987.

Stammer, D., C. Wunsch, R. Giering, Q. Zhang, J. Marotzke, J. Marshall, and C. Hill, The global ocean circulation estimated from TOPEX/POSEIDON altimetry and the MIT general circulation model, *Cent. Global Change Sci. Rep. Ser., 49* pp. 1–40, Mass. Inst. Technol., Cambridge, 1997.

Stommel, H., Determination of watermass properties of water pumped down from the Ekman layer to the geostrophic flow below, *Proc. Natl. Acad. Sci. U. S. A., 76* 3051–3055, 1979.

Tapley, B. D., D. P. Chambers, C. K. Shum, R. J. Eanes, J. C. Ries, and R. H. Stewart, Accuracy assessment of the large scale dynamic ocean topography from TOPEX/Poseidon altimetry, *J. Geophys. Res., 99,* 24,605–24,617,1994.

Williams, R. G., The influence of air-sea interaction on the ventilated thermocline, *J. Phys. Oceanogr., 19,* 1255–1267, 1989.

Williams, R. G., The role of the mixed layer in setting the potential vorticity of the main thermocline, *J. Phys. Oceanogr., 21,* 1803–1814, 1991.

Williams, R. G., M. A. Spall, and J. C. Marshall,1995 Does Stommel's mixed-layer "Demon" work?, *J. Phys. Oceanogr., 25,* 3089–3102, 1995.

Wunsch, C., Dynamically consistent hydrography and absolute velocity in the eastern North Atlantic Ocean, *J. Geophys. Res., 99,* 14,071 14,090, 1994.

Wunsch, C., and D. Roemmich, Is the North Atlantic in Sverdrup balance?, *J. Phys. Oceanogr., 15,* 1876–1880, 1985.

M. Pennington and R. G. Williams, Oceanography Laboratories, University of Liverpool, Liverpool, L69 3BX, England, UK. (ric@liv.ac.uk)

(Received July 29, 1998; revised February 22, 1999; accepted April 16, 1999.)